On the potential of healing metals through electrodeposition

P. Cavaliere[1], B. Bozzini[1], C. Mele[1], A. Taurisano[2]
[1]Dept. of Innovation Engineering, University of Salento, Via per Arnesano, I-73100 Lecce, Italy
pasquale.cavaliere@unisalento.it
[2]EnginSoft SpA, Via Antonio Murri 2, Zona Industriale, Mesagne, Brindisi 72023, Italy

Abstract
The proposed approach is based on electrodeposition into high aspect-ratio via and through-holes. The notch behavior of AA2099 is studied through Finite Element Analysis by employing ANSYS. The mechanical behavior of a V-notched aluminum panel is analyzed in the present study. The model is developed in order to predict the stress field coming from the combination of the two different materials repairing the panel through electrodeposited copper filling the notch. The electrodeposition shows a beneficial effect in terms of stress reduction around the notch. A study about the possibility to use the copper electrodeposition to repair a corrosion damaged surface is also performed.

Keywords:
Crack healing, FEM, electrodeposition, corrosion

1 INTRODUCTION

This paper intends to contribute to the essentially incipient research field of self-healing (SH) metallic materials. This topic has been recently reviewed in [1]. The seminal works in this field are essentially devoted to the following three types of materials. (i) Under-aged Al-Cu-based alloys, where SH is obtained at room temperature by precipitation [2-4]. (ii) SH of creep damage in austenitic stainless steel, achieved by the spontaneous deposition of B and BN inside creep cavities, suppressing that of S [5]. (iii) Metal-matrix composites reinforced by shape-memory alloy wires, achieving crack-closure thanks to shape recovery effects [6]. In this work we mean to launch an innovative approach, based on the sealing of existing cracks by bottom-up electrodeposition (ECD) [7]. This process has been demonstrated for Cu, but of course this metal gives rise to obnoxious galvanic coupling. Thus, in this specific paper, we address both mechanical and corrosion problems of a crack present in an AA2099 foil, filled with ECD Cu. ECD in this work has been in fact regarded as an ex situ conventional plating process; in this configuration, no actual SH process can be claimed. Nevertheless, ECD processes in principle can be tailored on the nanoscale and implemented by delivering the plating system in the form of vesicles containing the plating solution [7] and nanoparticles acting as sacrificial anodes. Appropriate functionalisation of the outer vesicle surface can lead to enhanced penetration into the crack and curvature-sensitive vesicle opening, eventually leading to the release of the plating system and to localised metal deposition inside the crack. This concept is being progressively developed in our group.

259 mm

2 MATERIALS AND METHODS

2.1 Al alloy and electrodeposition (ECD) process

AA2099 (Cu 2.7, Li 1.8, Zn 0.7, Mg 0.35, Mn 0.35, Zr 0.1, Ti 0.05, Fe 0.05, Si 0.03, Al bal. [8]) is an innovative Al-Li alloy for aerospace applications requiring high strength, low density, high stiffness, superior damage tolerance, excellent corrosion resistance and weldability. Cu has been electrodeposited from an acidic sulphate solution, containing the classical additives adopted for ULSI processes [9, 10].

2.2 Mechanical Computations by ANSYS

Using the ANSYS finite element code, a 3D finite element model was generated, consisting of isoparametric brick elements. In order to account for surface-to-surface contact and frictional sliding, we used the contact element CONTAC48. Three-phased unit cells with hexagonal symmetry were employed. Mixed-mode debonding conditions between the two materials were modeled by a bilinear cohesive law.

2.3 Corrosion Rate Distribution Computations

The 2D current density distributions have been computed by the COMSOL Multiphysics FEM solver V.3.5. In our computations we employed with Butler-Volmer boundary conditions in order to

simulate accurately the electrokinetics and deformable domains to follow the shape changes due to Al corrosion. The exchange current density for the non-linear boundary conditions corresponding to AA2099 corrosion has been calibrated with the experimental corrosion rate estimated from experiments detailed in Electrochemical Corrosion Measurements.

2.4 Corrosion Measurements

Electrochemical measurements were performed with an PAR Potentiostat. A three-electrode configuration was used. The counter-electrode was a large-area (10 cm2) Pt mesh electrode. The reference electrode was an Ag/AgCl (KCl 3M). Electrochemical impedance measurements have been carried out in the frequency range $5*10^{-3}$-10^{+5} Hz at open circuit potential with a sinusoid amplitude of 10 mV peak-to-peak.

3 RESULTS AND DISCUSSION

3.1 FEM mechanical computations

In order to optimize the stiffness and strength of the repaired material, a strong interface bond is required, resulting in high shear strength of the material and effective load transfer. For this reason, it is crucial to analyze the interface quality in terms of oxides formation and/or voidance. In view of this, two kind of electrodeposits were prepared: -Cu deposited on as-received, anodised 2099 sheets or after mechanochemical oxide removal. In the case of electrodeposition after removal of the oxide film (Figure 1), the ECD Cu layer appears more uniform and voids and defects can hardly be detected: in this case, typically corresponding to the surface conditions of the crack walls, the Al/Cu interface was modeled as perfectly bonded.

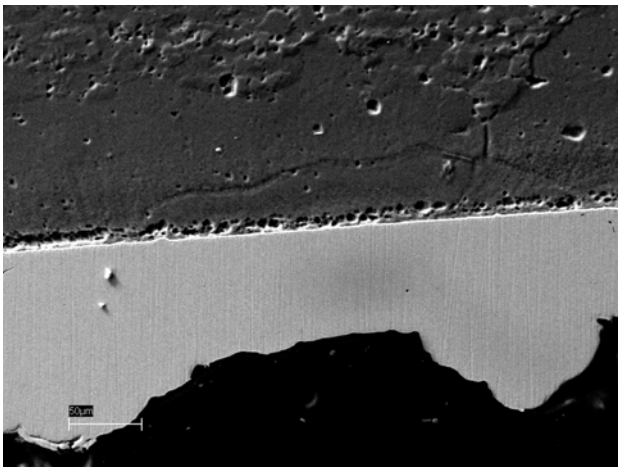

Figure 1: Cu electrodeposit on AA2099 without oxidation defects.

The 3D finite element model adopted in this work is shown in Figure 2. The size of the control volume was five times larger than that of the volume of interest (VOI) in Y- and Z-directions, so that boundary effects are minimised. Inside the VOI we locate the V-notch of the panel measuring 100 μm length with an angle of aperture of 30°. The sheet was fixed on one edge and subjected to uniform and constant loading on the free edge. In such way the crack experiences Mode I loading.

Since the Stress Intensity Factor (SIF) results are highly sensitive to the size of elements used near the crack tip, we adopted an optimised adaptive meshing procedure. Actually, the transfer of elastic stress predominates during initial loading, such transfer affects the overall behavior of the bulk structure, especially as far as damage initiation is concerned. Upon further deformation, the maximum stress zone moves from the crack tip to the surface. The Linear Elastic Fracture Mechanics (LEFM) approach was used as a means to evaluate the stress field caused by the presence either of the crack or of the Cu filling.

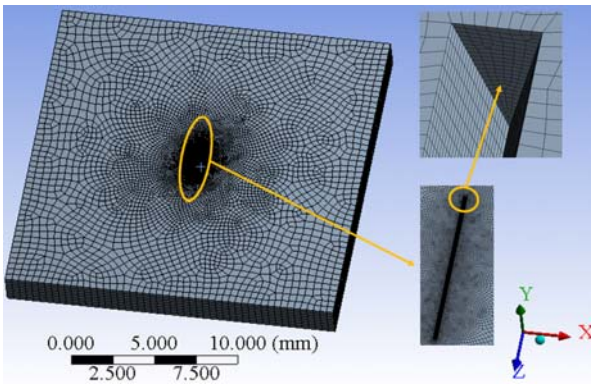

Figure 2: The 3D finite element model adopted in this work.

The stress fields around the crack tip obtained in the two cases were computed and compared. Figure 3a shows the radial nature of the maximum principal stress field in-plane, showing that the crack intensity factor exhibits a maximum value at the crack tip and decreases moving toward the sheet surface. The Von Mises stress, shown in Figure 3b, exhibits the same behavior as the SIF.

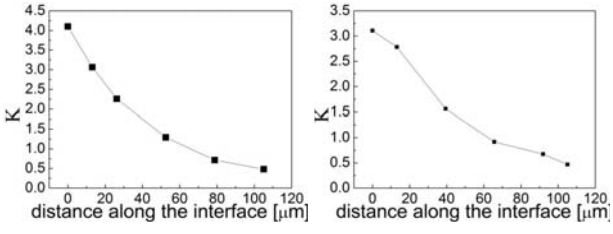

Figure 3: In-plane maximum principal (a) and VonMises (b) stress field for an open crack. Insets show the crack intensity factor as a function of distance from sheet surface.

If the crack is repaired by filling with ECD Cu, a notable change in principal (Figure 4a) and Von Mises (Figure 4b) stresses is found. Panels 4a and 4b in fact refer to the stress along the crack edge

from the tip to the surface, ratioed to that found at the center of the deposited Cu on the surface (low-stress zone). Figures 4c and 4d depict the same situation, but in this case the stress concentration is plotted as the ratio between: (i) the principal (Panel 4c) and Von Mises (Panel 4d) stresses, acting on the AA2099 in a volume very close to the Cu filling and (ii) the respective stresses computed in the Al bulk (low-stress zone). One can notice that: (i) with an open crack (Figure 3), the SIF shows its maximum at the crack tip and then it decreases moving along the side towards the sheet surface; (ii) on the contrary, in the case of a Cu-sealed crack (Figure 4), it exhibits its minimum at the crack tip and then it increases towards the sheet surface.

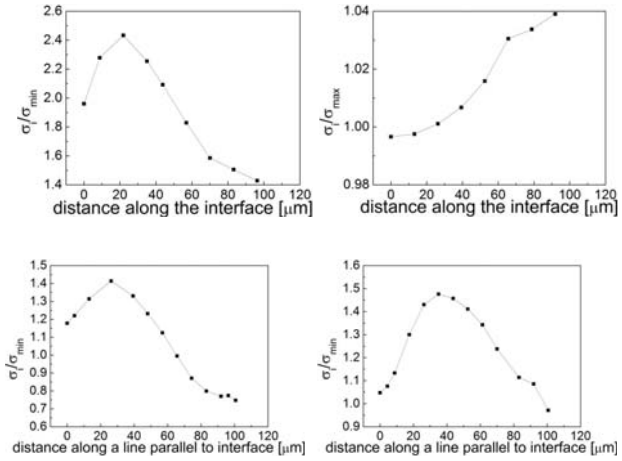

Figure 4: Maximum principal (a, c) and Von Mises (b, d) stress field in presence of Cu filling. (c) and (d) stress distributions in a section of the Al sheet, parallel to the Cu/Al interface. Insets highlight the dependence on the distance from the crack surface.

Figure 5 reports the relative values of maximum stresses at the same point within the Al bulk, obtained by ratioing the results obtained in the absence (σmax2209) and in the presence (σmax2209-Cu) of crack filling.

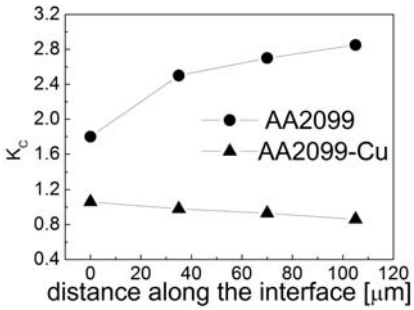

Figure 5: The ratios of the maximum stress in the absence (σmax2209) and in the presence (σmax2209-Cu) of crack filling.

3.2 Electrochemical Corrosion Measurements

The galvanic coupling between Al and Cu gives rise to anodic polarisation of the former metal, resulting in its preferential dissolution. A selection of electrochemical measurements was performed, employing AA2099 coupons as such and with ECD Cu layers (ca. 50 μm thick) covering half of the area exposed to the solution [11]. In order to emphasise corrosive criticalities, we performed corrosion testing in a strongly aggressive attack solution: aerated simulated seawater (NaCl 0.85 M, pH 7). We recorded the time-dependent open-circuit potential (OCP) and we measured electrochemical impedance spectrometry (EIS) at OCP. Zero-resistance ammetry (ZRA) measurements were carried out with a AA2099 coupon coupled with a pure Cu rod (Goodfellow). Figure 6a shows the evolution of OCP for the Al (A) and Al/Cu (B) coupons. The Al sample exhibits a slow drift towards slightly more noble potentials. To the contrary, the Au/Cu couple undergoes relatively fast denobling, corresponding to progressive activation of the corrosion process. The potential transient recorded during the ZRA measurement (Figure 6b) essentially confirms the OCP results of Figure 6a-B, while the current transient exhibits a progressive reduction of the current density due to the precipitation of corrosion products at the Al surface (pseudopassivation). The EIS spectra for AA2099 (A) and the AA2099/Cu (B) samples are shown in Figure 6c.

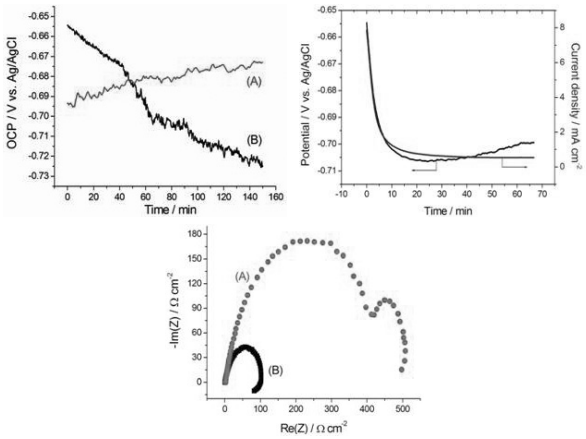

Figure 6: Open Circuit Potential (OCP) evolution for AA2099 without (A) and with (B) galvanic coupling to ECD Cu (a); ZRA measurements for the AA2099/Cu coupling (b); Electrochemical Impedance Spectra (EIS) at Open Circuit Potential for AA2099 without (A) and with (B) galvanic coupling to ECD Cu (c).

The overall faradaic resistance is decreased by a factor of 5 by coupling with Cu: this result matches quantitatively with the ZRA results, considering that the OCP is fixed at the beginning of the EIS measurement. Both spectra are characterised by two time constants. Both loops are capacitive for AA2099 (A): reasonably their resistive components

correspond to faradaic and oxide resistance. Instead, the capacitive low-frequency loop of the Al/Cu system (B) is inductive and denotes the fact that corrosion goes on with the mediation of an adsorbed intermediate, in keeping with the pseudo-passivating behaviour found by ZRA. Coupling with Cu gives rise to an overall enhancement of corrosion rate [12], but this is also accompanied by a self-limiting, pseudopassivating process related to the precipitation of corrosion products. ZRA and EIS measurements allow the estimation of a corrosion rate of ca. 0.6 μm h-1: this figure is about three order of magnitude higher than those reported as typical for Al alloys for marine applications, such as 1XXX and 5XXX [12].

3.3 Numerical evaluation of Morphology Evolution due to Galvanic Coupling

We simulated the time-dependent shape changes of the AA2099/Cu contact due to galvanic corrosion resulting from the presence of Cu wedges inserted into the Al sheet, forming angles of 30°, 60° and 90° to its surface. The integration domain for the pristine conditions are represented by a half-circle, centred at the contact point between the Cu wedge, simulating crack filling with ECD Cu and the Al surface (Figure 7-A).

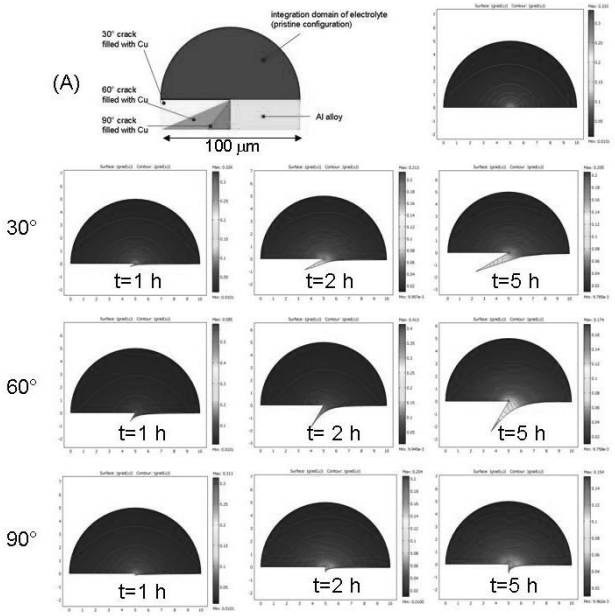

Figure 6: Open Circuit Potential (OCP) evolution for AA2099 without (A) and with (B) galvanic coupling to ECD Cu (a); ZRA measurements for the AA2099/Cu coupling (b); Electrochemical Impedance Spectra (EIS) at Open Circuit Potential for AA2099 without (A) and with (B) galvanic coupling to ECD Cu (c).

Insulating boundary conditions (BCs) are set on the semi-circle, corrosion BCs at the interface between Al and electrolyte and O2 reduction BCs at the Cu-electrolyte contact [13, 14]. The time-dependent Al consumption and formation of a gap at the Al/Cu contact have been simulated for three idealised crack geometries, corresponding to the crack penetrating into the Al surface at 30°, 60° and 90°, respectively. In Figure 7 we report the current density distribution for the three considered crack geometries (color-coded with red iso-current lines) and the attending shape evolution of the Al alloy resulting from the distribution of the corrosion rate. Corrosion is more severe at the Al/Cu interface and gives rise to a secondary crack which is function of the angle.

4 SUMMARY

Based on Cu ECD into high aspect-ratio vias and through-holes, developed for ULSI fabrication in electronics, Cu electroplating into cracks of metal items can be regarded as a feasible process. In this study we have investigated mechanical and corrosion aspects of filling cracks in AA2099 sheets by Cu ECD. The crack behavior of AA2099 was studied by FEM, employing ANSYS (Version 13.0). The study was finalized to predict the failure initiation locus in the case of repaired panels subjected to bending loading and deformation. We have quantified the way stress concentration, residual stress field and failure are affected by the mechanical properties of the constituent materials and by the geometrical and mechanical properties of the interface. Moreover, we have evaluated the residual stress field at the interface between aluminum and copper. The mechanical computational study was complemented by the experimental investigation of the Al/ECD Cu interface, based on SEM observation and EDX microanalysis measurements. Eventually, the corrosion behaviour resulting from the galvanic coupling of AA2099 and ECD Cu was studied experimentally by OCP, ZRA and EIS measurements, that provided quantitative corrosion rate estimates and mechanistic information. Precipitation of bulky corrosion products at the Al/Cu gap yields a self-inhibiting corrosion process, that reduces the attack rate of this chemically unfavourable material combination. Our results prove the conceptual feasibility of the process and its considerable mechanical advantages open up a novel, promising approach to crack path evolution.

5 REFERENCES

[1] Ghosh S.K. (ed). "Self-healing Materials - Fundamentals, Design Strategies, and Applications" Wiley-VCH Weinheim (D) 2009, Chapters 7 and 8.

[2] Lumley, R.N. Morton A.J. and Polmear, I.J. (2002) Acta Materialia 50, 3597–3608.

[3] Lumley, R.N. Schaffer, G.B. (2006) Scripta Materialia 55, 207–210.

[4] Hautakangas, S. Schut, H. van der Zwaag, S. Rivera Diaz del Castillo, P.E.J. and van Dijk, N.H. (2007) Physical Status Solidi C 4 (10), 3469–3472.

[5] Laha, K. Kyono, J. Sasaki, T. Kishimoto S. and Shinya N. (2005) Met. Mat. Trans. A 36, 399–409.

[6] Burton, D.S. Gao, X. and Brinson L.C. (2006) Mechanics of Materials 38, 525–537.

[7] Bozzini, B. D'Urzo, L. Mele, C. Busson B. and Tadjedine A. (2010) Trans. IMF 88, 130-143.

[8] Bois-Brochu, A., Goma, F.A.T., Blais, C., Larouche, D., Gauvin, R., Boselli, J. (2012) Adv. Mater. Research 409, 29-34.

[9] Bozzini, B. D'Urzo, L. Huo, S.J. Cai, W.B. (2008) Trans. IMF Finishing 86, 41-50.

[10] D'Urzo, L. Bozzini, B. (2009) Journal of Materials Science: Materials in Electronics 20 217-222.

[11] Gouveia-Caridade, C. Pereira, M.I.S. Brett, C.M.A. (2004) Electrochimica Acta 49, 785-783.

[12] Missert, N. Barbour, J.C. Copeland R.G. and Mikkalson, J.E. (2001) JOM 53 (7), 34-37.

[13] Giovannelli, G. D'Urzo, L. Maggiulli, G. Natali, S. Pagliara, C. Sgura, I. and Bozzini, B. (2010) J. Solid State Electrochem. 14, 479-494.

[14] Despic, A.R. In: Conway BE, Bockris JO'M, Yaeger E, Khan SUM, White RE (ed) Comprehensive Treatise of Electrochemistry, vol. 7, Plenum Press, (1983) NY.